Electron-Transfer Kinetics of Copper(II/I) Complexes with Dialcoholic Derivatives of the Macrocyclic Tetrathiaether [14]aneS$_4$. Effect of Simple Ring Substituents upon Gated Behavior

Nancy E. Meagher,[1a] Kerri L. Juntunen,[1a] Mary Jane Heeg,[1a] Cynthia A. Salhi,[1a] Brian C. Dunn,[1a] L. A. Ochrymowycz,[1b] and D. B. Rorabacher*,[1a]

Departments of Chemistry, Wayne State University, Detroit, Michigan 48202, and University of Wisconsin—Eau Claire, Eau Claire, Wisconsin 54701

Received July 8, 1993[⊗]

Studies have been conducted on the electron-transfer kinetics of the Cu(II/I) complexes formed with two dialcoholic derivatives of the macrocyclic tetrathiaether [14]aneS$_4$, *syn*- and *anti*-3,6,10,13-tetrathiacyclotetradecane-1,8-diol. For Cu$^{II/I}$(*syn*-[14]aneS$_4$-diol), the self-exchange rate constant has been determined directly from NMR line broadening: $k_{11(ex)} = 2.9 \times 10^3$ M^{-1} s^{-1} (25 °C), $\Delta H^* = 33 \pm 5$ kJ mol^{-1}, $\Delta S^* = -68 \pm 20$ J K^{-1} mol^{-1}. For both Cu$^{II/I}$L systems, extensive cross-reaction electron-transfer kinetics have also been measured using four different reductants and four different oxidants, spanning a wide range of reaction potentials. The patterns in the k_{11} values obtained by application of the Marcus square root relationship are consistent with the previously proposed dual-pathway square scheme mechanism in which both pathways have been accessed. Under appropriate conditions, limiting first-order kinetics, independent of the counter reagent concentration, have also been observed for the oxidation of both Cu^{I}L species, indicating the onset of conformationally-controlled "gated" behavior. The evaluated self-exchange rate constants representative of each pathway (i.e., $k_{11(A)}$ and $k_{11(B)}$ in units of M^{-1} s^{-1}) and the evaluated rate constant for the Cu^{I}L conformational change (k_{RP} in units of s^{-1}) are as follows at 25 °C and μ = 0.1 M: for the *syn* complex, log $k_{11(A)} = 3.6 \pm 0.2$, log $k_{11(B)} = -0.4 \pm 0.3$, and log $k_{RP} = 2.20 \pm 0.02$; for the *anti* complex, log $k_{11(A)} = 4.3 \pm 0.2$, log $k_{11(B)} = -2.0 \pm 0.4$, and log $k_{RP} = 1.70 \pm 0.03$. The 10^6-fold difference in the k_{11} values obtained for the two pathways in the latter system represents the widest range of conditions for gated behavior yet observed, suggesting that the Cu^{II}L metastable intermediate (Q) is particularly unstable relative to the Cu^{I}L metastable intermediate (P). Crystallographic structural data are also reported for each of the Cu^{II}L species. [Cu^{II}(*syn*-[14]aneS$_4$-diol)(ONO$_2$)]NO$_3$ crystallizes in the monoclinic space group $P2_1/a$ with $a = 9.238(1)$ Å, $b = 13.248(2)$ Å, $c = 15.321(2)$ Å, $\beta = 104.21(1)°$, $V = 1817.5(4)$ Å^3, $Z = 4$; [Cu^{II}(*anti*-[14]aneS$_4$-diol)](ClO$_4$)$_2$ crystallizes in the monclinic space group $P2_1/c$ with $a = 5.8472(9)$ Å, $b = 17.764(3)$ Å, $c = 9.601(1)$ Å, $\beta = 102.43(1)°$, $V = 973.8(2)$ Å^3, $Z = 2$.

Introduction

Extensive electron-transfer kinetic studies for both self-exchange[2] (eq 1) and cross-reactions[2] (eq 2) as well as electrochemical measurements[3] on Cu$^{II/I}$([14]aneS$_4$) have shown that

$$*Cu^{II}L + Cu^{I}L \underset{}{\overset{k_{11}}{\rightleftharpoons}} *Cu^{I}L + Cu^{II}L \qquad (1)$$

$$Cu^{II}L + A_{Red} \underset{k_{21}}{\overset{k_{12}}{\rightleftharpoons}} Cu^{I}L + A_{Ox} \qquad (2)$$

the electron-exchange behavior conforms to a dual-pathway square scheme mechanism (Figure 1) in which the electron-transfer step and conformational changes occur sequentially rather than concertedly. Additional studies on both the electron self-exchange and cross-reaction kinetics for the Cu(II/I) complexes involving closely related macrocyclic polythiaethers, including [13]aneS$_4$,[4] [15]aneS$_4$,[4] and [15]aneS$_5$,[5] support the contention that the dual-pathway mechanism is also applicable to other systems. We have suggested, in fact, that this may be a common mechanism for all Cu(II/I) systems.

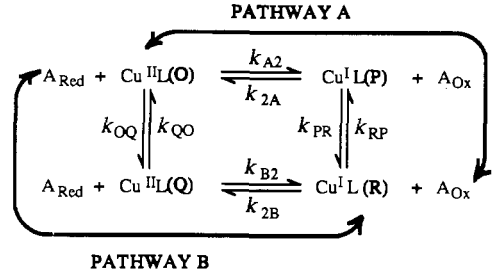

Figure 1. Proposed dual-pathway square scheme mechanism for Cu$^{II/I}$L electron transfer. In this scheme, O and R represent the stable forms of Cu^{II}L and Cu^{I}L, respectively, while the species designated as Q and P represent metastable intermediates which are presumed to resemble the conformations of the corresponding stable species for the opposite oxidation states.

The presence of two pathways, as depicted in Figure 1, is indicated experimentally by the appearance of two limiting values for k_{11}. If pathway A is nominally preferred (implying that intermediate Q is less stable that intermediate P), as appears to be the case for the polythiaether complexes examined to date, the self-exchange rate constant values calculated from experimental k_{12} values for Cu^{II}L reduction reactions ($k_{11(Red)}$) are constant regardless of the counterreagent utilized and are in agreement with the k_{11} value as determined directly for reaction 1 using NMR line-broadening measurements (designated as $k_{11(ex)}$);[2,4] by contrast, the k_{11} values calculated from experimental k_{21} values for Cu^{I}L oxidation ($k_{11(Ox)}$) tend to be variable with $k_{11(Ox)} \leq k_{11(ex)}$, ultimately reaching a lower limit representative of pathway B.[2,4] The "apparent" values for $k_{11(Ox)}$ are dependent on the relative contributions of the two individual pathways which, in

⊗ Abstract published in *Advance ACS Abstracts*, January 1, 1994.

(1) (a) Wayne State University. (b) University of Wisconsin—Eau Claire.
(2) Meagher, N. E.; Juntunen, K. L; Salhi, C. A.; Ochrymowycz, L. A.; Rorabacher, D. B. *J. Am. Chem. Soc.* **1992**, *114*, 10411-10420.
(3) (a) Bernardo, M. M.; Robandt, P. V.; Schroeder, R. R.; Rorabacher, D. B. *J. Am. Chem. Soc.* **1989**, *111*, 1224-1231. (b) Robandt, P. V.; Schroeder, R. R.; Rorabacher, D. B. *Inorg. Chem.* **1993**, *32*, 3957-3963.
(4) Leggett, G. H.; Dunn, B. C.; Vande Linde, A. M. Q.; Ochrymowycz, L. A.; Rorabacher, D. B. *Inorg. Chem.* **1993**, *32*, 5911-5918.
(5) Vande Linde, A. M. Q.; Juntunen, K. L.; Mols, O.; Ksebati, M. B.; Ochrymowycz, L. A.; Rorabacher, D. B. *Inorg. Chem.* **1991**, *30*, 5037-5042.

0020-1669/94/1333-0670$04.50/0

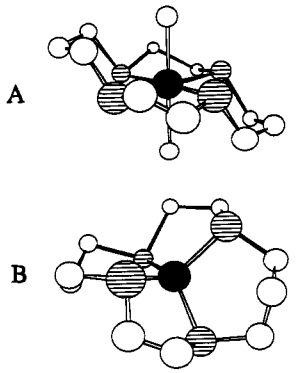

Figure 2. (A) Structure of $[Cu^{II}([14]aneS_4)(OClO_3)_2]$ as determined from X-ray crystallography[7b] showing the coplanarity of the Cu atom (solid) and the four sulfur donor atoms (shaded). In solution the axial positions are assumed to be occupied by water molecules (or possibly weakly coordinating anions). (B) Presumed structure of $Cu^{I}([14]aneS_4)$ based on the crystal structure of a closely related analogue, $[Cu^{I}([14]aneNS_3)]ClO_4$.[8]

turn, depend on the overall rate of reaction as influenced by the potential, self-exchange rate constant, and concentration of the counterreagent.

For reactions in which pathway A is preferred, theoretical considerations[6] have shown that, under intermediate conditions, oxidation reactions should exhibit electron-transfer kinetics which appear to be first order (independent of the concentration of counterreagent), indicating that the conformational change designated as R → P (Figure 1) has become rate limiting. However, of the Cu(II/I)–polythiaether systems which we have examined to date, only in the case of the $Cu^{II/I}([14]aneS_4)$ system has the latter limiting condition been observed.[2] For that specific system, in fact, the value of k_{RP} has also been corroborated from rapid-scan cyclic voltammetric studies.[3b] Since the magnitude of k_{RP} should reflect the relative influence of conformational constraints in the ligand structure, this latter constant is of especial interest. Therefore, we have sought to identify other related systems for which k_{RP} might be quantitatively determined.

The $[14]aneS_4$ ligand is known to be somewhat unique in that it is of optimal size to form a tetragonal complex with the Cu(II) ion in which the four thiaether sulfur donor atoms lie coplanar with the copper atom, and the elongated axial sites are occupied by solvent molecules or weakly coordinating anions[7] (Figure 2A). Although this ligand cannot readily adapt to a regular tetrahedral coordination geometry, as would presumably be preferred by Cu(I), the $Cu^{I}L$ species is very stable[8] and is believed to exist in solution as a 1:1 complex involving a flattened tetrahedral configuration[9] (Figure 2B).

In an attempt to gain some insight into the influence of steric factors upon the value of k_{RP} and the relative competitiveness of the two electron-transfer pathways, we have undertaken a study of the electron-transfer kinetics of the copper complexes formed with both *syn*- and *anti*-3,6,10,13-tetrathiacyclotetradeca-1,8-diol, otherwise designated as *syn*- and *anti*-$[14]aneS_4$-diol, respectively. Not only are these ligands closely related to $[14]aneS_4$ but they have the added advantage of being highly soluble in aqueous solution. Moreover, the stability constants and

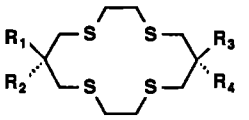

$R_1 = R_2 = R_3 = R_4 = H$: $[14]aneS_4$

$R_1 = R_3 = OH$; $R_2 = R_4 = H$: *syn*-$[14]aneS_4$-diol

$R_1 = R_4 = OH$; $R_2 = R_3 = H$: *anti*-$[14]aneS_4$-diol

formation rate constants for the $Cu^{II}L$ complexes formed with both diol ligands have also previously been determined,[10] differing significantly from the parent $[14]aneS_4$ complex. The *syn* isomer has also previously been shown to exhibit electrochemical behavior which is consistent with Figure 1.[3a] However, no direct measurements on the kinetics for electron self-exchange or cross-reactions with counterreagents have previously been reported with either diol complex.

As part of the current investigation, the crystallographic structures have been determined for the $Cu^{II}L$ complexes formed with the two diols and, at least in the solid state, reveal significant differences in conformation. The accompanying kinetic studies have been designed to explore the extent to which changes in ground state conformation might be manifested in the apparent self-exchange electron-transfer rate constants and the limiting rate constant for conformational change.

Experimental Section

Reagents. The synthesis of the isomeric mixture of *syn*- and *anti*-$[14]aneS_4$-diol and the procedure used for separating the two isomers have previously been reported.[10] Pure crystalline $Cu(ClO_4)_2$,[10] used as the copper salt in all cross reactions, copper(II) nitrate,[10] used for the NMR line-broadening studies, and copper metal shot[2] (99.90%, Allied Chemical Corp.), used for the reduction of $Cu^{II}L$ to the corresponding $Cu^{I}L$ species, were prepared and/or purified as previously described. For the ^1H NMR measurements on *syn*-$[14]aneS_4$-diol, deuterium oxide (99.8% D), used for all $Cu^{I}L$ spectra, and methanol-d_4 (99.5% D), used to obtain the free ligand spectrum, were purchased from Aldrich Chemical Co. For all other studies, distilled–deionized water was used as the solvent.

The preparation of seven of the counterreagents used in the current work has been previously described,[2,11] including $Ru^{II}(NH_3)_5py$, $Ru^{II}(NH_3)_5isn$, $Ru^{II}(NH_3)_4bpy$, $Ru^{III}(NH_3)_4bpy$, $Ru^{III}(NH_3)_2(bpy)_2$, $Ni^{III}([14]aneN_4)$, and $Fe^{III}(4,7\text{-}Me_2phen)_3$. [*Caution*! The perchlorate salts of the ruthenium complexes are potentially explosive! Such compounds should be prepared only in small quantities and should never be dried (other than air drying).] For these compounds, py = pyridine, isn = isonicotinamide, bpy = 2,2′-bipyridine, $[14]aneN_4$ = 1,4,8,11-tetraazacyclotetradecane, and 4,7-Me_2phen = 4,7-dimethyl-1,10-phenanthroline. In addition to these reagents, $Ru(NH_3)_4phen^{2+}$ (phen = 1,10-phenanthroline) was prepared as the trimethylsulfonate salt starting with $[Ru(NH_3)_5(H_2O)](CF_3SO_3)_2$ (as prepared by Diamond and Taube)[12] and using Brown and Sutin's method to convert to the final product.[13] The final extraction procedure was modified to utilize carbon tetrachloride rather than ether as the organic solvent, thereby improving the extraction efficiency since 1,10-phenanthroline is more soluble in carbon tetrachloride than in ether whereas the ruthenium salt is less soluble. Finally, bis(1,4,7-trithiacyclononane)cobalt(II) perchlorate, $[Co([9]aneS_3)_2](ClO_4)_2$, was prepared according to the method of Glass and co-workers[14] with the exception that cobalt(II) perchlorate was substituted for cobalt(II) acetate as a starting material. (*Caution*! Cobalt perchlorate salts are also potentially explosive.)

Preparation of Solutions. Solutions of the Cu^{I}(*syn*-$[14]aneS_4$-diol) and Cu^{II}(*syn*-$[14]aneS_4$-diol) complexes for the NMR studies were prepared in D_2O as previously described.[5] Since the Cu(II) complexes formed with both diol ligands are relatively weak,[10] a large excess of

(6) Hoffman, B. M.; Ratner, M. A. *J. Am. Chem. Soc.* **1987**, *109*, 6237–6243; **1988**, *110*, 8267.
(7) (a) Glick, M. D.; Gavel, D. P.; Diaddario, L. L.; Rorabacher, D. B. *Inorg. Chem.* **1976**, *15*, 1190–1193. (b) Pett, V. B.; Diaddario, L. L., Jr.; Dockal, E. R.; Corfield, P. W.; Ceccarelli, C.; Glick, M. D.; Ochrymowycz, L. A.; Rorabacher, D. B. *Inorg. Chem.* **1983**, *22*, 3661–3670.
(8) Bernardo, M. M.; Schroeder, R. R.; Ochrymowycz, L. A.; Rorabacher, D. B. *Inorg. Chem.* **1991**, *30*, 1241–1247. The $Cu^{I}([14]aneS_4)$ complex stability constant is very large (1.3×10^{12} M^{-1}) compared to that of $Cu^{II}([14]aneS_4)$ (2.2×10^{4} M^{-1}). [See: (a) Sokol, L. S. W. L.; Ochrymowycz, L. A.; Rorabacher, D. B. *Inorg. Chem.* **1981**, *20*, 3189–3195. (b) Young, I. R.; Ochrymowycz, L. A.; Rorabacher, D. B. *Inorg. Chem.* **1986**, *25*, 2576–2582.]
(9) See discussion in ref 4.
(10) Pett, V. B.; Leggett, G. H.; Cooper, T. H.; Reed, P. R.; Situmeang, D.; Ochrymowycz, L. A.; Rorabacher, D. B. *Inorg. Chem.* **1988**, *27*, 2164–2169.
(11) Martin, M. J.; Endicott, J. F.; Ochrymowycz, L. A.; Rorabacher, D. B. *Inorg. Chem.* **1987**, *26*, 3012–3022.
(12) Diamond, S. E.; Taube, H. *J. Am. Chem. Soc.* **1975**, *97*, 5921–5923.
(13) Brown, G. M.; Sutin, N. *J. Am. Chem. Soc.* **1979**, *101*, 883–892.
(14) Setzer, W. N.; Ogle, C. A.; Wilson, G. S.; Glass, R. S. *Inorg. Chem.* **1983**, *22*, 266–271.

Cu^{2+}(aq) was added to all solutions containing $Cu^{II}L$ to ensure essentially complete formation of the complex.

Instrumentation. Cyclic voltammograms, used for determining the formal potential values of the $Cu^{II/I}L$ redox couples, were generated using a Bioanalytical Systems BAS-100 electrochemical analyzer equipped with a glassy-carbon-disk working electrode, a platinum-wire auxiliary electrode, and a Ag/AgCl reference electrode (containing 3 M NaCl, for which E^f = 0.197 V vs NHE).[15] All kinetic measurements for electron-transfer cross reactions were made using a Durrum Model D-110 stopped-flow spectrophotometer which was interfaced to an Eltech Turbo XT computer equipped with a Metrabyte 12 bit A/D board. Visible absorption measurements for all solutions were made using a Cary 17D double-beam recording spectrophotometer. Measurements of pH were made using an Orion Model 901A digital ionalyzer equipped with a micro Ag/AgCl pH combination electrode. A Nicolet GN 300 MHz spectrometer, equipped with a variable temperature unit and a Nicolet NMC 1280 data system, was used for all ^1H NMR measurements.

NMR Measurements. A one-pulse-sequence was used for the acquisition of the free induction decay (FID) signal for all line-broadening experiments on Cu^{I}(*syn*-[14]aneS$_4$-diol). Shimming on the FID was used to ensure a homogeneous field. The following parameters were employed in this study: 40 pulses, 10-μs pulse length, 1.5-s delay time, 1.64-s acquisition time, sweep width (SW) = ±2500 Hz, and block size = 16 K. Six samples containing constant amounts of $Cu^{I}L$, but varying concentrations of $Cu^{II}L$ were prepared for each series of measurements. Each NMR tube was stoppered with a rubber septum to minimize air oxidation during the line-broadening measurements, and the NMR spectrum for each tube was recorded at four temperatures (5, 15, 25, and 35 °C). The inversion recovery (T1IR) method was used for T_1 relaxation measurements.[16] In resolving the "doublet" peak in the vicinity of 3.3 ppm, the Curve Analysis Program (CAP)[17] was used. Following completion of the NMR measurements, the specific concentration of $Cu^{II}L$ in each solution was determined by transferring the solution from the NMR tube to a small volume 1-cm cell and measuring the absorbance at 390 nm.

Crystallography. Single-crystal X-ray diffraction experiments were performed on a Syntex P2$_1$ automated diffractometer with Mo Kα radiation and a graphite monochromator at ambient temperature. The structures were solved by Patterson or direct methods and refined in full matrices with the programs of SHELX-76.[18] All non-hydrogen atoms were refined anisotropically. Hydrogen atoms were placed in observed positions and held invariant or refined. Neutral atom scattering factors and corrections for anomalous dispersion were from ref 19. Absorption corrections were made by empirical methods.[20] Crystallographic experimental parameters are given in Table 1.

Results

Determination of $Cu^{II/I}L$ Potential Values. The formal potential values for the two $Cu^{II/I}L$ systems were determined at ambient temperature (≈22 °C) from slow-scan cyclic voltammetry (CV) on solutions which contained 0.10 M $NaClO_4$, approximately 5 × 10^{-4} M $Cu^{II}L$, and 0.033 M $Cu(ClO_4)_2$, the large excess of Cu^{2+}(aq) being added to ensure complete complexation of the $Cu^{II}L$ complex. The CV curves were well-behaved and yielded $E_{1/2}$ values which were constant (within ± 0.8 mV) over the scan range of 1–500 mV s^{-1}. The resultant potential values for the two isomeric complexes are listed in Table 2 where they are compared to the parent [14]aneS$_4$ system. Also listed in this table are the stability constants previously determined for the $Cu^{II}L$ complexes[10] and the corresponding values for the $Cu^{I}L$ complexes as calculated from the Nernst equation based on the measured potential values.[21]

Table 1. Crystallographic Data for [Cu^{II}(*syn*-[14]aneS$_4$-diol)(ONO$_2$)]NO$_3$ (**1**) and [Cu^{II}(*anti*-[14]aneS$_4$-diol)](ClO$_4$)$_2$ (**2**)

	1	**2**
formula	$CuS_4O_8N_2C_{10}H_{20}$	$CuCl_2S_4O_{10}C_{10}H_{20}$
fw	488.08	562.97
space group	$P2_1/a$	$P2_1/c$
a, Å	9.238(1)	5.8472(9)
b, Å	13.248(2)	17.764(3)
c, Å	15.321(2)	9.601(1)
β, deg	104.21(1)	102.43(1)
V, Å^3	1817.5(4)	973.8(2)
Z	4	2
ρ (calc), g cm^{-3}	1.784	1.920
λ, Å	0.71073	0.71073
T, °C	22	22
μ, cm^{-1}	16.85	18.59
transm factors	0.592–0.524	0.637–0.594
R^a	0.036	0.040
R_w^b	0.043	0.044

^{a} $R = (\Sigma||\Delta F|)/(\Sigma|F_o|)$. ^{b} $R_w = [\Sigma w|\Delta F|^2)/\Sigma w(F_o)^2]^{1/2}$.

Table 2. Apparent Formal Potential Values for the Cu(II/I)–Polythiaether Systems Included in This Work and the Individual Stability Constants of the $Cu^{II}L$ and $Cu^{I}L$ Species in Aqueous Solution at 25 °C and μ = 0.10 M

complexed ligand	E^f, V vs NHE[a]	$K_{Cu^IL'}/K_{Cu^{II}L'}$ calcd[b]	$K_{Cu^{II}L'}$ exptl	$K_{Cu^IL'}$ calcd
[14]aneS$_4$	0.58[c]	4.0×10^7	2.18×10^4 [d]	8.8×10^{11}
syn-[14]aneS$_4$-diol	0.540(1)[e,f]	8.5×10^6	1.3×10^3 [g]	1.1×10^{10}
anti-[14]aneS$_4$-diol	0.489(1)[e,f]	1.2×10^6	7.8×10^3 [g]	9.4×10^9

[a] All formal potential values were derived from slow scan (1–500 mV s^{-1} sweep rate) cyclic voltammetric measurements assuming $E^f \approx E_{1/2}$ (see text). [b] Calculated from the Nernst equation as previously described in ref 3. [c] Reference 2. [d] Sokol, L. S. W. L.; Ochrymowycz, L. A.; Rorabacher, D. B. *Inorg. Chem.* **1981**, *20*, 3189–3195. [e] Potential measured at ambient temperature (≈22 °C), μ = 0.20 M (0.10 M $NaClO_4$ + 0.033 M $Cu(ClO_4)_2$, is assumed to approximate the value at 25 °C, μ = 0.1 M. [f] For this and the following tables, numbers given in parentheses represent the standard deviation for the preceding value in terms of the last digit(s) listed, e.g., 0.540(1) represents 0.540 ± 0.001. [g] Reference 10.

Stopped-Flow Kinetic Studies. Each of the $Cu^{II}L$ complexes included in this work was reacted with four reductants with a known propensity for undergoing outer-sphere electron-transfer reactions. These reagents were selected to provide a significant range of potentials: $Ru^{II}(NH_3)_4$bpy, $Ru^{II}(NH_3)_4$phen, $Ru^{II}(NH_3)_5$isn, and $Ru^{II}(NH_3)_5$py. A fifth reductant, $Co^{II}([9]aneS_3)_2$, was utilized to reduce Cu^{II}(*syn*-[14]aneS$_4$-diol) but was found to provide unsatisfactory results due to rapid complex dissociation of the cobalt complex under the conditions used. The corresponding $Cu^{I}L$ species were also reacted with four oxidants which were selected on a similar basis: $Ru^{III}(NH_3)_4$bpy, Ni^{III}([14]-aneN$_4$)(H$_2$O)$_2$, $Ru^{III}(NH_3)_2(bpy)_2$, and Fe^{III}(4,7-Me$_2$phen)$_3$. The literature values for the potentials and the self-exchange rate constants for these reagents are listed in Table 3. Also included in this table are the contact radii for each reactant species as utilized in later calculations.

As indicated by the data in Table 3, nearly all cross-reaction rate constants obtained in this work had values of 10^5 M^{-1} s^{-1} or larger, ranging up to 10^7 M^{-1} s^{-1}. To permit a reasonably accurate evaluation of these very large rate constants, most reactions were studied under conditions where neither reagent was present in large excess (i.e., pseudo-first-order conditions were avoided). Under these circumstances, all reactions, except those with Ni^{III}([14]aneN$_4$), were found to conform to the reversible second-order expression

$$dX/dt = k_{12}[A][B] - k_{21}[C][D] \quad (3)$$

where the terms [A], [B], [C], and [D] represent the molar concentrations of $Cu^{II}L$, A_{Red}, $Cu^{I}L$, and A_{Ox}, respectively, at any time, t (see reaction 2). As has been previously shown,[2]

(15) Bard, A. J.; Faulkner, L. R. *Electrochemical Methods*; Wiley: New York, 1980; p 720.
(16) Freeman, R.; Kempsell, S. P.; Levitt, M. H. *J. Magn. Reson.* **1980**, *38*, 453–479.
(17) *NMC-1280 Manual*; Nicolet Magnetics Corporation: Freemont, CA, 1982.
(18) Sheldrick, G. M. SHELX-76. University Chemical Laboratory, Cambridge, England, 1976.
(19) *International Tables for X-Ray Crystallography*; Kynoch: Birmingham, England, 1974; Vol. 4 (present distributor: D. Reidel, Dordrecht, The Netherlands).
(20) Sheldrick, G. M. SHELXTL. University of Göttingen, Germany, 1978.
(21) Bernardo, M. M.; Heeg, M. J.; Schroeder, R. R.; Ochrymowycz, L. A.; Rorabacher, D. B. *Inorg. Chem.* **1992**, *31*, 191–198.

Table 3. Second-Order Electron-Transfer Rate Constants Obtained for Reactions of $Cu^{II/I}$(*syn*-[14]aneS$_4$-diol) and $Cu^{I/I}$(*anti*-[14]aneS$_4$-diol) Using Selected Counterreagents in Aqueous Solutions at 25 °C and μ = 0.10 M (ClO_4^-)

reagent	E^f, V	k_{22}, M^{-1} s^{-1}	$r \times 10^8$, cm	k_{12} (or k_{21}) $\times 10^{-5}$, M^{-1} s^{-1} for Cu complex	
				syn-[14]aneS$_4$-diol	*anti*-[14]aneS$_4$-diol
			Reductants		
$Ru^{II}(NH_3)_4$bpy	0.526[a]	2.2×10^6 [b]	4.4[c]	1.34(3)	1.46(17)
$Ru^{II}(NH_3)_4$phen	0.515[d]	2.2×10^6 [e]	4.4[e]	2.11(15)	1.26(17)
$Co^{II}([9]aneS_3)_2$	0.42[f]	1.6×10^5 [g]	4.3[f]	11.8(14)	
$Ru^{II}(NH_3)_5$isn	0.387[h]	1.1×10^5 [i]	3.8[i]	6.6(3)	5.2(4)
$Ru^{II}(NH_3)_5$py	0.32[a]	1.1×10^5 [b]	3.8[b]	16.5(10)	15.6(16)
			Oxidants		
$Ru^{III}(NH_3)_4$bpy	0.526[a]	2.2×10^6 [b]	4.4[c]	0.19(2)	0.82(5)
$Ni^{III}([14]aneN_4)(H_2O)_2$	0.95[j-l]	1.0×10^3 [j-l]	3.6[l]	[8.3(6)][m]	[16.6(10)][m]
$Ru^{III}(NH_3)_2bpy_2$	0.889[n]	8.4×10^7 [b]	5.6[b]	43(2)	18(8)
Fe^{III}(4,7-Me$_2$phen)$_3$	0.939[c]	3.3×10^8 [o]	6.6[c]	116(34)	48(5)

[a] Yee, E. L.; Weaver, M. J. *Inorg. Chem.* **1980**, *19*, 1077–1079. [b] Reference 13. [c] Reference 11. [d] Endicott, J. F.; Durham, B.; Kumar, K. *Inorg. Chem.* **1982**, *21*, 2437–2444. [e] The value of k_{11} is assumed to be identical to that for the corresponding bipyridyl complex: $Ru(NH_3)_4bpy^{3+/2+}$. [f] Küppers, H.-J.; Neves, A.; Pomp, C.; Ventur, D.; Wieghardt, K.; Nuber, B.; Weiss, J. *Inorg. Chem.* **1986**, *25*, 2400–2408. [g] Küppers, H.-J.; Wieghardt, K.; Steenken, S.; Nuber, B.; Weiss, J. *Z. Anorg. Allg. Chem.* **1989**, *573*, 43–62. [h] Stanbury, D. M.; Haas, O.; Taube, H. *Inorg. Chem.* **1980**, *19*, 518–524. [i] The value of k_{11} is assumed identical to that for the corresponding pyridyl complex: $Ru^{III/II}(NH_3)_5$py. [j] Haines, R. I.; McAuley, A. *Coord. Chem. Rev.* **1981**, *39*, 77–119. [k] McAuley, A.; Macartney, D. H.; Oswald, T. *J. Chem. Soc., Chem. Commun.* **1982**, 274–275. [l] Fairbank, M. G.; Norman, P. R.; McAuley, A. *Inorg. Chem.* **1985**, *24*, 2639–2644. [m] Values shown are apparent second-order rate constants from initial studies; the reactions are actually first order, being independent of $Ni^{III}([14]aneN_4)$ over an extended concentration range (see text). [n] Seddon, E. A.; Seddon, K. R. *The Chemistry of Ruthenium*; Elsevier: New York, 1984; p 444. [o] Ruff, I.; Zimonyi, M. *Electrochim. Acta* **1973**, *18*, 515–516.

appropriate substitutions into eq 3 lead to the following integrated expression:[22]

$$\frac{[C]_e[D]_e}{\sqrt{b^2-4ac}}\left\{\ln\left(\frac{2aX_t+b-\sqrt{b^2-4ac}}{2aX_t+b+\sqrt{b^2-4ac}}\right)-\ln\left(\frac{2aX_0+b-\sqrt{b^2-4ac}}{2aX_0+b+\sqrt{b^2-4ac}}\right)\right\}=k_{12}t \quad (4)$$

where the parameters in eq 4 are defined as follows:

$$a = [C]_e[D]_e - [A]_e[B]_e$$

$$b = -\{([A]_0 + [B]_0)[C]_e[D]_e + ([C]_0 + [D]_0)[A]_e[B]_e\}$$

$$c = [A]_0[B]_0[C]_e[D]_e - [A]_e[B]_e[C]_0[D]_0$$

$$X_0 = [A]_i - [A]_0 = [B]_i - [B]_0 = [C]_0 - [C]_i = [D]_0 - [D]_i$$

The quantities with subscripts "e" and "i" represent the final concentrations at equilibrium (i.e., at infinite time) and immediately after mixing (prior to reaction initiation), respectively.

Equation 4 corrects for any contribution from the back reaction and is sensitive to any products initially present at the time of reaction initiation. Thus, it is very sensitive to changing conditions. In the case of $Cu^{I}L$ solutions, the presence of some air oxidation could be detected by the increasing coloration of the solution within the drive syringe as a function of time. Corrections for such oxidation were made by arbitrarily "tweaking" the initial concentration value until an optimal fit to eq 4 was obtained. Such concentration corrections, when made, were always small (less than 10%) and were in the direction anticipated for air oxidation.[23] The results of the second-order rate constants obtained in this manner were in agreement with the results obtained under pseudo-first-order conditions for systems in which both types of studies were made. The use of eq 4 provided satisfactory kinetic plots for even the most rapid reactions included in this work.

Table 4. Experimentally Determined Cross-Reaction Rate Constants for the Oxidation of Cu^{I}(*syn*-[14]aneS$_4$-diol) with $Ni^{III}([14]aneN_4)$ as a Function of Reagent Concentration in Aqueous Solution at 25 °C and μ = 0.2 M ($HClO_4$)

[Ni(III)], mM	$k_{21} \times 10^{-4}$, M^{-1} s^{-1}	[Ni(III)], mM	$k_{21} \times 10^{-4}$, M^{-1} s^{-1}
	Series I: $[Cu^{I}L]$ = 32.2 μM		
0.50	46.0	2.00	9.24
1.00	16.1	4.00	5.00, 6.22
	Series II: $[Cu^{I}L]$ = 38.3 μM[a]		
0.464	11.7	1.39	5.25
0.696	7.32	1.62	4.49
0.928	6.02	1.86	3.24
1.16	6.09	2.09	3.37
	Series III: $[Cu^{I}L]$ = 227 μM		
0.886	20.6	3.14	8.46
0.932	22.3	6.36	5.87
1.55	13.1		
	Series IV: $[Cu^{I}L]$ = 22.7 μM		
0.232	43.2	3.14	8.46
0.432	40.8	6.36	6.26
1.55	15.1		

[a] Series II data differ statistically from the other series and are not included in Figure 7.[35]

For each of the reactions studied, at least three sets of reagent solutions were prepared in which the reactant concentrations were varied slightly. For each series, at least six repetitive runs were made for which the calculated k_{12} (or k_{21}) values were statistically averaged (see supplementary material). The mean rate constant value for each reaction studied is included in Table 3. Also included in this table for comparison are the corresponding values previously reported for the parent system, $Cu^{II/I}([14]aneS_4)$.

As in our previous study on the cross-reaction kinetics for $Cu^{II/I}([14]aneS_4)$,[2] the kinetics for the oxidation of each of the diol complexes using $Ni^{III}([14]aneN_4)$ as the oxidant gave evidence of limiting first-order kinetic behavior. Therefore, extensive kinetic studies were conducted under pseudo-first-order conditions (Ni(III) in excess) in which the $Ni^{III}([14]aneN_4)$ concentration was varied over a range of approximately 50-fold. The results of these studies are listed in Tables 4 and 5 where the pseudo-

(22) Smith, J. M. *Chemical Engineering Kinetics*, 2nd ed.; McGraw-Hill: New York, 1970; pp 60–65.

(23) The integrity of these so-called "tweaking" corrections could be checked by filling the cell manually with the $Cu^{I}L$ solution from the drive syringe and noting the increase in absorbance, as a function of time, due to the appearance of $Cu^{II}L$. It was also noted that, in all cases, sucessively larger corrections were required with each successive repetitive run and that the use of these corrections resulted in consistent rate constant values for the repetitive runs. Whenever the corrections exceeded about 10%, the drive syringes were refilled with fresh solution before continuing.

(24) As noted in the Discussion, these "apparent" second-order rate constants contain both first- and second-order components. Such "apparent" second-order rate constants, while unconventional, are exactly analogous in their connotation to "apparent" (or "pseudo" or "observed") first-order rate constants for reactions which may contain second-order components.

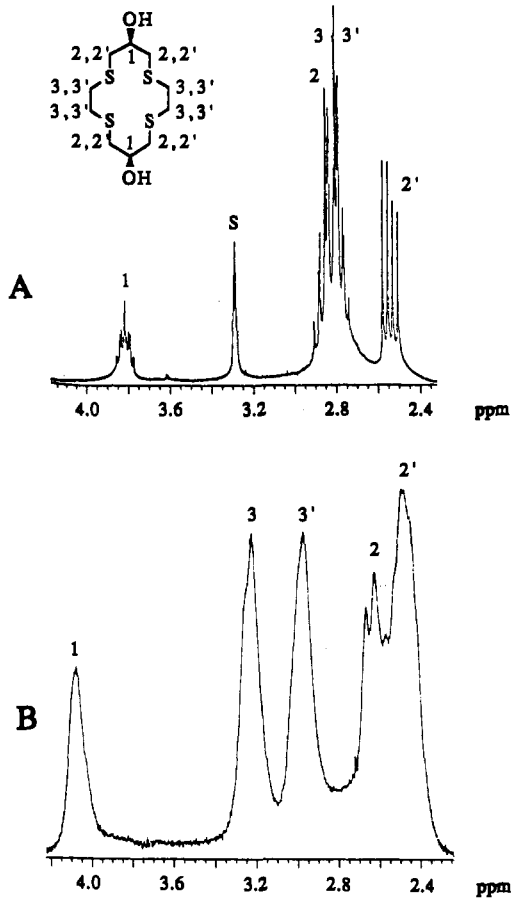

Figure 3. ^{1}H spectra for (A) the uncomplexed *syn*-[14]aneS$_4$-diol ligand in CD_3OD and (B) the Cu^I(*syn*-[14]aneS$_4$-diol) complex in D_2O. Peak assignments are shown for both spectra, the peak labeled S in spectrum A being attributable to the solvent.

Table 5. Experimentally Determined Cross-Reaction Rate Constants for the Oxidation of Cu^I(*anti*-[14]aneS$_4$-diol) with Ni^{III}([14]aneN$_4$) as a Function of Reagent Concentration in Aqueous Solution at 25 °C and μ = 0.10 (ClO_4^-)

[Ni(III)], mM	$k_{21} \times 10^{-4}$, M^{-1} s^{-1}	[Ni(III)], mM	$k_{21} \times 10^{-4}$, M^{-1} s^{-1}
	Series I: [Cu^{I}L] = 9.89 μM		
0.120	34.8	0.837	5.62
0.239	21.0	1.20	4.31
	Series II: [Cu^{I}L] = 40.0 μM		
0.307	18.2	1.54	4.58
0.404	14.1	2.69	2.85
0.594	9.38	3.84	2.31
0.768	8.43	4.99	1.87
0.997	5.63	6.15	1.54

first-order rate constants have been divided by the concentration of the Ni(III) reagent to yield "apparent" second-order rate constants.[24]

NMR Measurement of Self-Exchange Rate Constant. The ^{1}H NMR spectrum of the free *syn*-[14]aneS$_4$-diol ligand in CD_3OD is shown in Figure 3A. The ^{13}C NMR spectrum was also acquired using "distortionless enhancement by polarization transfer" (DEPT)[25] with a pulse angle, $D\theta$, equal to 135°. This indicated that the methine carbon, to which the hydroxide group is attached, generated the peak furthest downfield (70 ppm). In the proton spectrum, the three analyte multiplets result in relative areas of 1:6:2. To correlate these ^{1}H peaks with those in the ^{13}C spectrum, a 2D experiment was performed. This confirmed the assignment of the peak at ca. 3.8 ppm to the two protons on the methine carbons. Decoupling experiments permitted the assignment of the remaining proton peaks.

The ^{1}H spectrum for the Cu^I(*syn*-[14]aneS$_4$-diol) complex in D_2O is shown in Figure 3B. The relative areas of the broad bands are in the ratio 1:2:2:4. Comparisons to the free ligand spectrum, in addition to the area ratios, support the premise that the peak at 4.1 ppm is due to the protons on the C-1 carbon. Decoupling experiments did not provide sufficient results to identify unequivocally the remaining peaks, presumably because the protons on C-2 (designated as H-2 and H-2′) are strongly influenced by the Cu(I) center, thus minimizing the effect of the decoupling process. In addition, it is apparent that, upon complexation, the original ligand symmetry is lost so that the four H-2′ protons are nonequivalent as are the four H-2 protons. From T_1 relaxation measurements, it was apparent that the null time for the methylene protons, H-2,2′ and H-3,3′, was 225 ms while that of the methine protons, H-1, was 550 ms. Therefore, the pulse delay time was set to 1.5 s for all NMR measurements for this system.

After optimal conditions had been established in an extensive series of preliminary experiments, the line-broadening measurements were made using two series of solutions having similar variations in complex concentration and pD. For each series of solutions, linewidth measurements were made at four temperatures: 5, 15, 25, and 35 °C. Two spectral regions were monitored in each line-broadening study: (i) the singlet at ca. 4.1 ppm assigned to the H-1 protons and (ii) the "doublet" centered at about 3.1 ppm attributed to the H-3 and H-3′ protons. In deconvoluting the latter "doublet", the precision was enhanced by assigning equal heights and areas to each of the resolved peaks. Each deconvolution was repeated five times and the mean line width was recorded.

As previously discussed,[2,5,26] the line width data were plotted according to the relationship derived by McConnell and Berger[27]

$$W_{DP}\mathcal{Q}\pi = W_D\mathcal{Q}\pi + k_{11(ex)}[Cu^{II}L] \qquad (5)$$

where W_{DP} represents the peak width at half-height of a resolved proton resonance peak for a solution containing both Cu^{I}L and Cu^{II}L, W_D represents the corresponding peak width for a solution containing only Cu^{I}L, and $\mathcal{Q}$ represents a correction term for the extent of outer-sphere contact pair formation as corrected to 0.1 M ionic strength.[5,28] Plots of the line-width data at all four temperatures for the singlet peak at about 4.1 ppm and for the resolved "doublet" in the region of 3.1 ppm are presented in parts A and B of Figure 4, respectively.[29] A summary of the $k_{11(ex)}$ values resolved from all four data sets is presented in Table 6 along with the values of $\Delta H^{\ddagger}$ and $\Delta S^{\ddagger}$ calculated from the temperature dependence.

(25) Doddrell, D. M.; Pegg, D. T.; Bendall, M. R. *J. Magn. Reson.* **1982**, *48*, 323–327.

(26) Vande Linde, A. M. Q.; Westerby, B. C.; Ochrymowycz, L. A.; Rorabacher, D. B. *Inorg. Chem.* **1993**, *32*, 251–257.

(27) McConnell, H. M.; Berger, S. B. *J. Chem. Phys.* **1957**, *27*, 230–234.

(28) In ref 5 and in the current work, a large excess of aquacopper(II) ion was added to prevent significant dissociation of the Cu^{II}L species. The presence of Cu^{II}(aq) caused significant NMR line broadening due to the paramagnetic effect, but this contribution to the line width was constant throughout the series of measurements and does not affect the slope. The very small self-exchange rate constant for the Cu$^{II/I}$(aq) system (10^{-5}–10^{-7} M^{-1} s^{-1}) precludes any significant contribution of this couple to the overall electron-transfer kinetics: Sisley, M. J.; Jordan, R. B. *Inorg. Chem.* **1992**, *31*, 2880–2884.

(29) The methine singlet decreases in width as the temperature is increased. This represents typical behavior for an NMR peak which is due to equivalent protons or protons involved in a conformational exchange in the fast exchange regime. These line width changes, combined with the increases in line width associated with the increasing rate of electron exchange as the temperature is raised, produce an overlapping pattern of intercepts as seen in Figure 4A. In contrast, the methylene doublet due to the H-3 and H-3′ protons is expected to merge with increasing temperatures as the rate of conformational exchange increases, indicative of the slow exchange regime. The result is an increase in the line width of each component of the doublet as the temperature is raised. The sum of this effect plus the line width increase with increasing rate of electron transfer leads to a large enhancement in intercept as the temperature increases as illustrated in Figure 4B. In either case, the line width effect due to conformational exchange is constant at constant temperature and, therefore, is not a factor in determining the slopes from which the $k_{11(ex)}$ values are calculated.

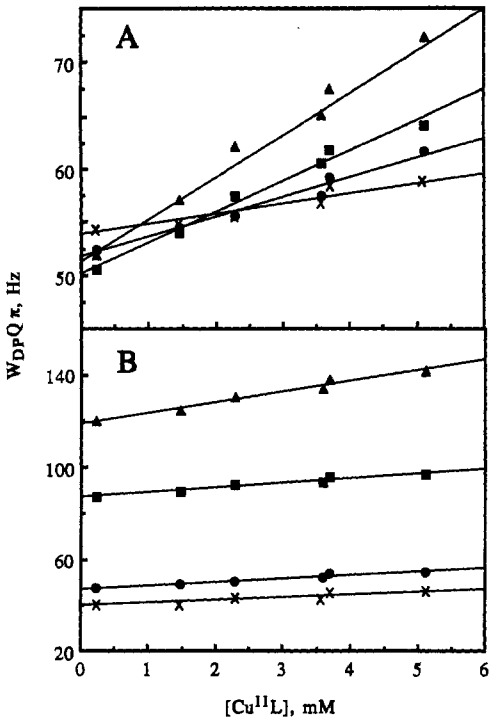

Figure 4. Plot of eq 5 for the NMR line broadening of (A) the methine H-1 singlet and (B) the methylene H-3,3′ doublet in the Cu^{I}(*syn*-[14]-aneS$_4$-diol) ^{1}H spectrum as a function of the concentration of added Cu^{II}(*syn*-[14]aneS$_4$-diol). Data shown are for series I: (×) 5 °C; (●) 15 °C; (■) 25 °C; (▲) 35 °C.[29]

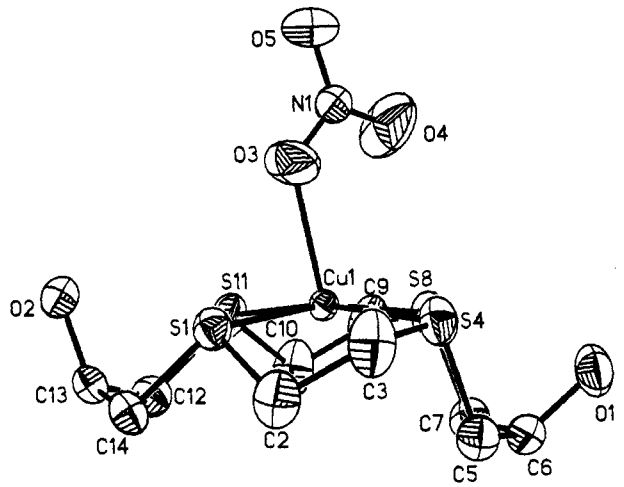

Figure 5. ORTEP drawing of the [Cu^{II}(*syn*-[14]aneS$_4$-diol)(ONO$_2$)] cation showing the atom numbering scheme. The Cu atom sits 0.22 Å above the plane of the four sulfur donor atoms. Note that the two –OH groups are nonequivalent in their orientation.

Table 6. Summary of Self-Exchange Rate Constant Data Resolved from NMR Line-Broadening Measurements on the Cu$^{II/I}$(*syn*-[14]aneS$_4$-diol) System in Aqueous Solution as Corrected to μ = 0.10 M (NO_3^-)[a]

	$k_{11} \times 10^{-3}$, M^{-1} s^{-1}			
peak monitored	5 °C	15 °C	25 °C	35 °C
methine singlet (series I)	0.9(2)	1.9(2)	2.9(2)	4.2(3)
methine singlet (series II)	0.9(1)	1.3(1)	3.1(1)	5.0(4)
methylene doublet (series I)	1.1(1)	1.5(1)	2.1(2)	4.6(4)
methylene doublet (series II)	1.0(1)	1.3(1)	2.0(1)	4.0(4)

[a] Mean activation parameters: $\Delta H^{\ddagger}$ = 33 ± 5 kJ mol^{-1}; $\Delta S^{\ddagger}$ = –68 ± 20 J K^{-1} mol^{-1}.

Structure Determination of the Cu^{II}-diol Complexes. The structure of [Cu^{II}(*syn*-[14]aneS$_4$-diol)(ONO$_2$)]NO$_3$ consists of one independent cation and one independent nitrate anion with all atoms occupying general positions. There are no unusual close contacts between residues. Fractional atomic coordinates are listed in Table 7. The atom labeling scheme for the cation is shown in Figure 5 and the bond lengths and angles are included in Table 8. In the [Cu^{II}(*syn*-[14]aneS$_4$-diol)(ONO$_2$)] unit, the copper atom lies in a square pyramidal environment being coordinated to the four sulfur donor atoms and a nitrate oxygen atom, with the copper lying 0.219 Å above the S$_4$ plane. This displacement of the Cu atom is reflected in the S–Cu–S bond angles involving the *trans* sulfur atoms: 167.96° for S1–Cu–S8 and 169.48° for S4–Cu–S11. As shown in Figure 5, all four

Table 7. Atomic Positional Parameters for [Cu^{II}(*syn*-[14]aneS$_4$-diol)(ONO$_2$)]NO$_3$

atom	*x*	*y*	*z*
Cu1	0.09573(5)	0.50733(3)	0.22519(3)
S1	0.1336(1)	0.34218(7)	0.27331(7)
S4	0.0709(1)	0.55190(8)	0.36784(8)
S8	0.1061(1)	0.67915(8)	0.19754(7)
S11	0.1642(1)	0.47458(7)	0.09327(7)
C2	0.2028(6)	0.3607(4)	0.3934(3)
C3	0.0948(7)	0.4300(4)	0.4251(4)
C5	0.2512(5)	0.6114(3)	0.4146(3)
C6	0.2614(5)	0.7150(3)	0.3753(3)
O1	0.1361(4)	0.7710(2)	0.3865(2)
C7	0.2772(5)	0.7169(4)	0.2785(3)
C9	0.1653(8)	0.6785(4)	0.0929(4)
C10	0.2657(7)	0.5922(4)	0.0862(4)
C12	0.3199(5)	0.3871(4)	0.1112(4)
C13	0.2867(5)	0.2851(3)	0.1464(3)
O2	0.1482(3)	0.2491(2)	0.0933(2)
C14	0.2941(5)	0.2839(3)	0.2465(3)
O3	–0.1383(4)	0.4518(3)	0.1716(3)
O4	–0.2193(5)	0.5955(3)	0.1289(3)
O5	–0.3683(4)	0.4692(3)	0.1083(3)
N1	–0.2442(4)	0.5075(3)	0.1376(2)
O6	0.6340(5)	0.3823(3)	0.3569(3)
O7	0.4854(4)	0.5052(3)	0.3098(3)
O8	0.7185(5)	0.5308(3)	0.3635(4)
N2	0.6119(5)	0.4727(3)	0.3440(3)

Table 8. Bond Lengths and Bond Angles for [Cu^{II}(*syn*-[14]aneS$_4$-diol)(ONO$_2$)]NO$_3$

Bond Lengths (Å)			
Cu1–S1	2.308(1)	C5–C6	1.510(6)
Cu1–S4	2.329(1)	C6–O1	1.420(5)
Cu1–S8	2.322(1)	C6–C7	1.526(5)
Cu1–S11	2.3022(9)	C9–C10	1.492(8)
Cu1–O3	2.240(3)	C12–C13	1.514(6)
S1–C2	1.810(4)	C13–O2	1.420(5)
S1–C14	1.806(4)	C13–C14	1.518(5)
S4–C3	1.825(5)	O3–N1	1.233(5)
S4–C5	1.823(5)	O4–N1	1.202(5)
S8–C7	1.824(5)	O5–N1	1.234(5)
S8–C9	1.816(4)	O6–N2	1.222(5)
S11–C10	1.836(5)	O7–N2	1.235(6)
S11–C12	1.815(5)	O8–N2	1.228(6)
C2–C3	1.521(7)		
Bond Angles (deg)			
Cu1–S1–C14	113.6(1)	Cu1–O3–N1	123.6(3)
Cu1–S1–C2	100.6(2)	S1–Cu1–S4	89.01(4)
Cu1–S4–C3	101.5(1)	S1–Cu1–S8	167.96(4)
Cu1–S4–C5	100.8(1)	S1–Cu1–S11	92.81(3)
Cu1–S8–C7	102.3(2)	S4–Cu1–S8	86.60(3)
Cu1–S8–C9	101.0(2)	S4–Cu1–S11	169.48(5)
Cu1–S11–C10	98.4(2)	S8–Cu1–S11	89.54(3)
Cu1–S11–C12	111.5(1)	S1–Cu1–O3	82.12(9)
S4–Cu1–O3	96.81(9)	C10–S11–C12	98.8(2)
S8–Cu1–O3	109.53(9)	C5–C6–C7	115.6(3)
S11–Cu1–O3	93.70(9)	C12–C13–C14	114.0(3)
S1–C14–C13	112.9(3)	C5–C6–O1	107.1(3)
S1–C2–C3	108.1(3)	C7–C6–O1	112.6(3)
S4–C3–C2	113.1(3)	C12–C13–O2	109.2(3)
S4–C5–C6	112.1(3)	C14–C13–O2	112.6(3)
S8–C7–C6	112.5(3)	O3–N1–O4	118.2(4)
S8–C9–C10	113.1(3)	O3–N1–O5	118.5(4)
S11–C10–C9	108.1(4)	O4–N1–O5	123.0(4)
S11–C12–C13	113.6(3)	O6–N2–O7	120.9(4)
C14–S1–C2	100.6(2)	O6–N2–O8	118.9(4)
C3–S4–C5	101.7(2)	O7–N2–O8	120.2(4)
C7–S8–C9	101.7(2)		

Table 9. Atomic Positional Parameters for [Cu^{II}(*anti*-[14]aneS$_4$-diol)](ClO$_4$)

atom	*x*	*y*	*z*
Cu1	1.00000	0.00000	0.00000
S1	1.1759(2)	−0.06988(7)	0.1960(1)
S4	0.7313(2)	0.04715(7)	0.1246(1)
C2	0.936(1)	−0.0678(3)	0.2902(5)
C3	0.8577(9)	0.0118(3)	0.3031(5)
C5	0.808(1)	0.1467(3)	0.1338(6)
C6	0.964(1)	0.1694(3)	0.0343(6)
C7	0.851(1)	0.1651(3)	−0.1229(6)
O1	1.1715(6)	0.1245(2)	0.0576(4)
Cl1	1.5577(2)	−0.16406(8)	0.5547(1)
O2	1.3124(7)	−0.1704(3)	0.5237(5)
O3	1.6506(9)	−0.2121(4)	0.6668(5)
O4	1.615(1)	−0.0903(3)	0.5883(9)
O5	1.641(1)	−0.1841(4)	0.4396(6)

Table 10. Bond Lengths and Bond Angles for [Cu^{II}(*anti*-[14]aneS$_4$-diol)](ClO$_4$)$_2$

	Bond Lengths (Å)		
Cu1–S1	2.303(1)	C5–C6	1.510(7)
Cu1–S4	2.326(1)	C6–C7	1.513(6)
Cu1–O1	2.443(3)	C6–O1	1.429(6)
S1–C7′	1.824(5)	Cl1–O2	1.405(4)
S1–C2	1.826(5)	Cl1–O3	1.389(6)
S4–C3	1.826(4)	Cl1–O4	1.374(6)
S4–C5	1.821(5)	Cl1–O5	1.348(5)
C2–C3	1.499(8)		
	Bond Angles (deg)		
Cu1–S1–C7′	101.5(2)	S4–C5–C6	113.8(3)
Cu1–S1–C2	97.9(2)	C7′–S1–C2	101.4(2)
Cu1–S4–C3	100.2(2)	C3–S4–C5	104.1(2)
Cu1–S4–C5	100.9(2)	C5–C6–C7	115.2(4)
Cu1–O1–C6	100.1(3)	C5–C6–O1	111.2(4)
S1–Cu1–S4	90.35(4)	C7–C6–O1	107.5(4)
S4–Cu1–S1′	89.65(4)	O2–Cl1–O3	109.0(3)
S1–Cu1–O1	102.34(8)	O2–Cl1–O4	108.1(3)
S4–Cu1–O1	81.21(8)	O2–Cl1–O5	109.8(4)
S1–C7′–C6″	114.4(3)	O3–Cl1–O4	111.7(4)
S1–C2–C3	109.9(4)	O3–Cl1–O5	108.8(4)
S4–C3–C2	108.4(3)	O4–Cl1–O5	109.4(4)

alkylene bridging groups are bent down away from the apical nitrate group with the two alcoholic oxygens bent upward. The resulting structure is analogous to the structure obtained earlier for [Cu^{II}([13]aneS$_4$)(OH$_2$)](ClO$_4$)$_2$[7b] except that, with the smaller ring, the Cu atom was displaced further (0.38 Å) above the S$_4$ plane.

Although the chelate bite angles for the ethylene-bridged sulfurs in the [Cu^{II}(*syn*-[14]aneS$_4$-diol)(ONO$_2$)] cation are in the expected range and are nearly equal (89.01° for S1–Cu–S4 and 89.54° for S8–Cu–S11), there is an unexpected skewing in the S$_4$ plane as shown by the disparate chelate bite angles for the sulfur atoms bridged by the two propylene groups: 86.60° for S4–Cu–S8 and 92.81° for S1–Cu–S11. As a result, the two alcoholic oxygen atoms are asymmetrically oriented relative to the S$_4$ plane (Figure 5). This is apparently a consequence of the mirror-like symmetry in the orientation of the two ethylene bridges which places differing strains on the two trimethylene bridges as the latter attempt to orient themselves on the same side of the S$_4$ plane. The result is reflected in the four S–Cu–O bond angles: S1–Cu–O, 82.12°; S4–Cu–O, 96.81°; S8–Cu–O, 109.53°; S11–Cu–O, 93.70°.

The asymmetric unit in the structure of [Cu^{II}(*anti*-[14]aneS$_4$-diol)](ClO$_4$)$_2$ consists of an independent half-cation and one independent anion. There are no unusual close contacts between residues. Fractional atomic coordinates are listed in Table 9. Bond lengths and angles for the cation are presented in Table 10.

The atomic labeling scheme for the [Cu^{II}(*anti*-[14]aneS$_4$-diol)] cation is shown in Figure 6A. In this unit, the Cu atom lies coplanar with the four sulfur donor atoms, and the arrangement of these five atoms is very similar to that found in the parent Cu^{II}([14]aneS$_4$) complex[7a] with the notable exception that the

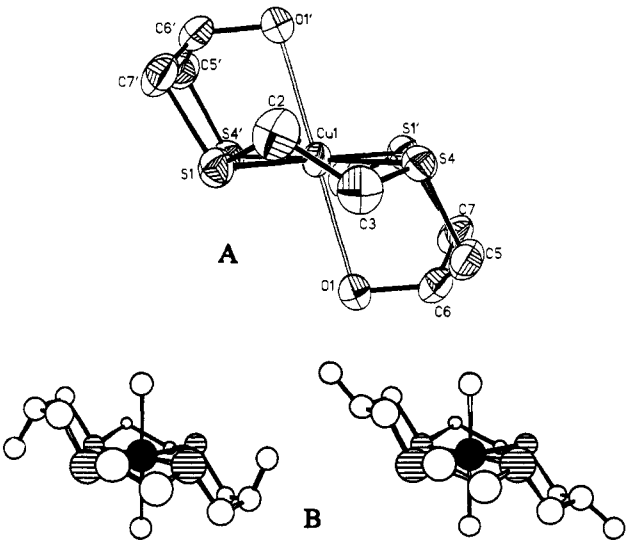

Figure 6. (A) ORTEP drawing of the [Cu^{II}(*anti*-[14]aneS$_4$-diol)]$^{2+}$ cation showing the atom numbering scheme. Note the coplanarity of the copper atom and the four sulfur donor atoms as well as the displacement of the axial oxygens from the perpendicular. (B) Alternate structures for the Cu^{II}(*anti*-[14]aneS$_4$-diol) complex in which solvent molecules (or anions) occupy the axial sites with the –OH groups uncoordinated. The latter structures are presumed to predominate in solution.

chelate bite angle for the propylene bridged sulfurs, 90.35°, is slightly larger than the corresponding angle for the ethylene bridged sulfurs, 89.65°. This phenomenon is undoubtedly caused by the fact that the hydroxy groups on the propylene bridges are being pulled toward the apical positions above and below the Cu atom as a result of Cu–O bonding interactions as reflected in the 2.443-Å distance between these atoms. Due to the constraints imposed by the ligand, the oxygen atoms are unable to achieve perpendicular apical positions as reflected by the acute S–Cu–O chelate bite angles: S1–Cu–O1′, 81.21°; S4–Cu–O1′, 79.66°. The Cu–O1 vector makes an angle of 74.8(5)° with the Cu–S$_4$ plane, a distortion which is clearly evident in the side view shown in Figure 6A. In comparing this structure to that of Cu^{II}([14]-aneS$_4$) in Figure 2, it should be noted that the central carbon atom in the propylene bridging group, when unconstrained in the [14]aneS$_4$ complex, is oriented in a chair, rather than a boat, configuration. Otherwise, all bond angles and distances are surprisingly consistent for the two compounds as noted in Table 10. In solution, it is expected that the axial sites in the *anti*-diol complex will be occupied by solvent molecules or weakly coordinated anions (Figure 6B), similar to the structure previously determined for Cu^{II}([14]aneS$_4$)[7a] (Figure 2A).

The torsion angles for both Cu(II)–diol complexes are listed in Table 11. The corresponding angles for the parent [Cu^{II}-([14]aneS$_4$)(ClO$_4$)$_2$] compound are also included in this table for comparison.

Discussion

Calculation of Apparent Self-Exchange Rate Constants. The counterreagents utilized in the cross-reaction kinetic studies were generally selected to promote an outer-sphere electron-transfer mechanism. Therefore, it is presumed that the Marcus cross relationship can be applied to each cross-reaction rate constant, k_{12} or k_{21}, in order to calculate the apparent value of the $Cu^{II/I}L$ self-exchange rate constant, k_{11}:[30]

$$k_{11} = \frac{(k_{12})^2}{k_{22}K_{12}f_{12}(W_{12})^2} \qquad (6)$$

In this expression, k_{22} represents the self-exchange rate constant

(30) (a) Marcus, R. A. *J. Chem. Phys.* **1956**, *24*, 966–978. (b) Marcus, R. A. *Discuss. Faraday Soc.* **1960**, *29*, 21–31. (c) Marcus, R. A. *J. Chem. Phys.* **1965**, *43*, 679–701. (d) Marcus, R. A.; Sutin, N. *Biochim. Biophys. Acta* **1985**, *811*, 265–322.

Table 11. Comparative Torsion Angles for $[Cu^{II}(syn\text{-}[14]aneS_4\text{-}diol)(ONO_2)]NO_3$ (1), $[Cu^{II}(anti\text{-}aneS_4\text{-}diol)](ClO_4)_2$ (2), and $[Cu^{II}([14]aneS_4)(ClO_4)_2]$ (3)

	torsion angle, deg[a]		
	1	2[b]	3[b]
S1–C2–C3–S4	−58.1(4)	65.7(4)	66.7(2)
S8–C9–C10–S11	59.9(5)	*−65.7(4)*	*−66.7(2)*
S1–C14–C13–C12	75.6(4)	*76.4(5)*	*−74.6(3)*
S4–C5–C6–C7	−73.3(4)	67.4(5)	−76.7(3)
S8–C7–C6–C5	70.9(5)	−76.4(5)	74.6(3)
S11–C12–C13–C14	−78.5(4)	*−67.4(5)*	*76.7(3)*
S1–C14–C13–O2	−49.6(4)	*−48.1(5)*	
S4–C5–C6–O1	53.2(4)	−55.1(5)	
S8–C7–C6–O1	−52.7(4)	48.1(5)	
S11–C12–C13–O2	48.5(4)	*55.1(5)*	
C2–S1–C14–C13	−164.0(3)	*102.8(4)*	*169.0(2)*
C3–C2–S1–C14	167.8(3)	−155.1(3)	−158.6(2)
C2–C3–S4–C5	−70.5(4)	−146.4(4)	−153.8(2)
C3–S4–C5–C6	178.7(3)	117.5(4)	117.4(2)
C6–C7–S8–C9	−175.2(3)	−102.8(4)	−169.0(2)
C7–S8–C9–C10	72.4(5)	*155.1(3)*	*158.6(2)*
C9–C10–S11–C12	−166.9(3)	*146.4(4)*	*153.8(2)*
C10–S11–C12–C13	163.6(3)	*−117.5(4)*	*−177.4(2)*

[a] In comparing the differences in torsion angles between two compounds, the sign is not significant since both hands are present in the crystal.[b] For compounds **2** and **3**, which lie on inversion centers, the torsion angles in italics are duplicates which are listed for purposes of comparison with compound **1**.

Table 12. Resolved Self-Exchange Rate Constants for $Cu^{II/I}([14]aneS_4)$, $Cu^{II/I}([syn\text{-}[14]aneS_4\text{-}diol)$ and $Cu^{II/I}(anti\text{-}[14]aneS_4\text{-}diol)$ as Calculated Utilizing the Marcus Relationship from Cross-Reaction Rate Constants Obtained with Selected Counterreagents in Aqueous Solution at 25 °C

	calcd log k_{11} (M^{-1} s^{-1}) for $Cu^{II/I}L$ Systems		
reagent	[14]aneS$_4$	*syn*-[14]aneS$_4$-diol	*anti*-[14]aneS$_4$-diol
	Direct Self-Exchange		
(NMR line-broadening)	3.81, 3.94[a]	3.40	
	Reductants		
$Co^{II}Z(H_2O)_2$[b]	3.24[c]		
$Ru^{II}(NH_3)_4bpy$	3.79[a]	3.50	4.23
$Ru^{II}(NH_3)_4phen$		3.59	4.08
$Ru^{II}(NH_3)_5isn$	4.02[a]	3.89	4.43
$Ru^{II}(NH_3)_5py$	3.89[a]	3.72	4.39
	Oxidants		
$Ru^{III}(NH_3)_4bpy$	2.58[a,d]	2.04[d]	2.68[d]
$Ni^{III}([14]aneN_4)(H_2O)_2$	2.44[e]	[2.63][e]	[2.54][e]
		lim: −0.7[f]	lim: −2.5[f]
$Ru^{III}(NH_3)_2(bpy)_2$	0.063[a]	−0.15	−1.77
$Fe^{III}(4,7\text{-}Me_2phen)_3$	0.20, −0.17[c] −0.38[a]	−0.24	−1.86

[a] Reference 2. [b] Z represents 2,3,9,10-tetramethyl-1,4,8,11-tetraazacyclotetradeca-1,3,8,10-tetraene ([Me_4[14]tetraeneN$_4$). [c] Reference 11. [d] Apparent value as calculated from initial data (see text). [e] Value calculated from initial "apparent" second-order rate constant; extended studies confirmed the fact that reaction is first order (independent of oxidant) over a wide concentration range. [f] Value of self-exchange rate constant for pathway B as calculated from apparent second-order cross-reaction rate constant extrapolated to high oxidant concentrations (see text).

of the counterreagent (as listed in Table 3), K_{12} represents the equilibrium constant for reaction 2, f_{12} is a nonlinear correction term, and W_{12} is the electrostatic work term (the latter terms having been defined previously).[11] (Note: For application to k_{21} values, all subscripts should be transposed.) The logarithmic values of k_{11} calculated from the use of eq 6 are listed in Table 12 for all reactions studied with both diol systems. The previously reported values for the parent system, $Cu^{II/I}([14]aneS_4)$, are also included for comparison.

For each of the three Cu(II/I) systems listed in Table 12, the log $k_{11(Red)}$ values are seen to be internally consistent within experimental error. Moreover, these $k_{11(Red)}$ values are also in excellent agreement with the $k_{11(ex)}$ values determined directly from NMR line-broadening measurements for the two systems for which such measurements have been obtained (Table 12). This behavior is consistent with that of other Cu(II/I)–polythiaether systems which we have previously studied in detail,[4,5,26] and adds further support to our proposal that, in the absence of conformationally-limiting conditions, Cu(II/I) systems exhibit behavior consistent with the Marcus relationship, contrary to some previous claims.[31]

For all three systems, however, the calculated $k_{11(Ox)}$ values in Table 12 are smaller than the $k_{11(Red)}$ values by as much as $3^1/_2$–6 orders of magnitude. As has been noted in our previous discussion of the $Cu^{II/I}([14]aneS_4)$ system,[2] this behavior is consistent with the mechanism depicted in Figure 1 for systems in which pathway A is preferred, the rate of the oxidation reactions being dependent upon the relative rates for the electron-transfer step and the conformational change (designated by rate constant k_{RP} in Figure 1). The intermediate $k_{11(Ox)}$ values obtained for the initial studies using $Ru^{III}(NH_3)_4bpy$ and $Ni^{III}([14]aneN_4)$ as the oxidants suggest that these specific reactions were in the intermediate region in which conformational change may be controlling the reaction rate. The observation of such intermediate behavior, along with differing values for $k_{11(Red)}$ and $k_{11(Ox)}$, is characteristic of the square scheme mechanism.[2]

Limiting Kinetic Behavior for Oxidation. As we have noted earlier,[2] application of the steady-state approximation to the two metastable intermediates, Q and P, yields the overall kinetic expression shown in eq 7 for $Cu^{I}L$ *oxidation* conforming to Figure

$$-\frac{d[Cu^{I}L]}{dt} = \left(\frac{k_{2A}k_{RP}}{k_{2A}[A_{Ox}] + k_{PR}} + \frac{k_{2B}k_{QO}}{k_{B2}[A_{Red}] + k_{QO}}\right)[R][A_{Ox}] \quad (7)$$

1 (where [R] is the concentration of the stable form of $Cu^{I}L$, and $[A_{Ox}]$ is the concentration of the counterreagent). Three limiting expressions are pertinent:[2]

$$-\frac{d[Cu^{I}L]}{dt} = K_{PR}^{-1}k_{2A}[R][A_{Ox}] \quad (7a)$$

$$-\frac{d[Cu^{I}L]}{dt} = k_{RP}[R] \quad (7b)$$

$$-\frac{d[Cu^{I}L]}{dt} = k_{2B}[R][A_{Ox}] \quad (7c)$$

Equation 7a (in which $K_{PR}^{-1} = k_{RP}/k_{PR}$) represents the situation where electron transfer occurs via pathway A with species R and P completely equilibrated (i.e., the conformational equilibrium is rapidly established relative to the rate of the electron-transfer step) while eq 7c represents the corresponding situation in which electron transfer occurs via pathway B with species O and Q completely equilibrated. Under either of these limiting conditions, the observed second-order behavior is completely indistinguishable from a single pathway mechanism, and the presence of the metastable intermediates is not apparent. Equation 7b represents the special situation in which pathway A is preferred but the conformational transformation of R → P has become rate-limiting, resulting in "gated" electron transfer.[6]

If the same pathway were being followed for both reduction and oxidation with the same set of limiting conditions, the values of $k_{11(Ox)}$ should be virtually identical to those of $k_{11(Red)}$ and $k_{11(ex)}$. Such behavior has recently been demonstrated for $Cu^{II/I}([13]aneS_4)$ and $Cu^{II/I}([15]aneS_4)$ when oxidants with small values of $K_{12}k_{22}$ (the "potential barrier function")[2] were utilized.[4] Since all of the $k_{11(Ox)}$ values obtained in this investigation are

(31) (a) Lee, C. W.; Anson, F. C. *J. Phys. Chem.* **1983**, *87*, 3360–3362. (b) Lee, C. W.; Shin, D. S.; Chair, T. S.; Kim, K. *Bull. Korean Chem. Soc.* **1991**, *12*, 454–455.

significantly smaller than the $k_{11(Red)}$ and $k_{11(ex)}$ values, it is apparent that eq 7a does not apply to any of the oxidation reactions included in Table 12. In fact, of the cross-reactions involving $Cu^{I}L$ oxidation, the calculated values for $k_{11(Ox)}$ are smallest for the reactions involving the largest values of $K_{21}k_{22}$, as has been observed in our two previous studies of this type.[2,4]

Gated Electron-Transfer Behavior. Of the oxidizing agents utilized, $Ru^{III}(NH_3)_4bpy$ and $Ni^{III}([14]aneN_4)$ have the smallest "potential barrier function" values and should come closest to fulfilling the requirements for eq 7a. As noted previously,[2] the reactions with the former reagent are thermodynamically unfavorable. This severely limits the range of conditions that can be accessed.[32] In the case of reactions with Ni(III), however, extensive concentration studies have revealed the presence of limiting first-order kinetics for all three Cu(II/I) systems reacting with this reagent, indicating that these oxidations were conducted under conditions where the rate of transformation of R → P has become rate limiting as described by eq 7b.

According to the theoretical treatment for square scheme mechanisms of the type shown in Figure 1, the $k_{B2}[A_{Red}]$ term in the denominator of the second parenthetical term in eq 7 will never be significant for thermodynamically favorable reactions.[33] Thus, the expression for the observed k_{21} values obtained with $Ni^{III}([14]aneN_4)$ can be reduced to a combination of one first-order term and two second-order terms

$$k_{21} = \frac{k_{2A}k_{RP}}{k_{2A}[A_{Ox}] + k_{PR}} + k_{2B} \qquad (8)$$

for which the three individual limiting conditions are represented in eq 7a–c. As the concentration of the Ni(III) reagent is varied, however, a mixture of two (or even all three) terms may contribute to the observed k_{21} values in some ranges. By operating under pseudo-first-order conditions, in which the concentration of $Ni^{III}([14]aneN_4)$ has been kept in large excess, we have avoided the possibility that the relative contributions of first- and second-order processes would change during the course of a single run. As noted earlier, the resulting pseudo-first-order rate constant values have been divided by the molar concentration of the Ni(III) reagent to generate *apparent* second-order rate constants,[24] thereby allowing these values to be compared directly to eq 8 (see Tables 4 and 5).

For conditions under which it was assumed that the second- and first-order terms in pathway A were the two dominant contributors to the observed kinetics, we have previously plotted the k_{21} data utilizing the inverse of the first term in eq 8,[2,34]

$$\frac{1}{k_{21}} = \frac{[A_{Ox}]}{k_{RP}} + \frac{K_{PR}}{k_{2A}} \qquad (8a)$$

Applying this expression to the two diol systems results in plots which begin to level off at $[Ni^{III}([14]aneN_4)] \geq 1$ mM. Such behavior indicates that the k_{2B} term is becoming appreciable.

In the concentration range in which the k_{2B} term becomes appreciable, we may assume, as a first approximation, that the second-order contribution to pathway A is not significant (i.e., $k_{RP} \ll k_{2A}[A_{Ox}]$). On the basis of this premise, an alternate limiting form of eq 8 may be utilized at high Ni(III) concentrations:

$$k_{21} = \frac{k_{RP}}{[A_{Ox}]} + k_{2B} \qquad (8b)$$

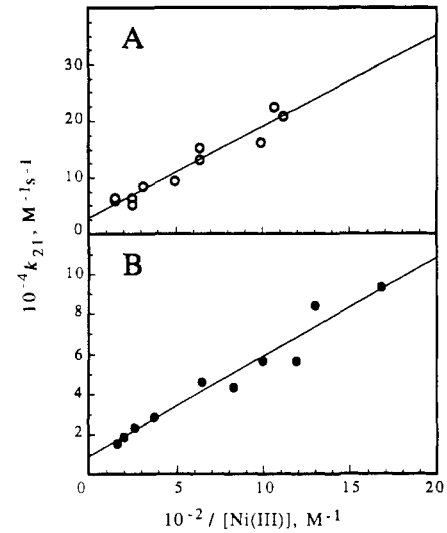

Figure 7. Plot of eq 8b for the "apparent" second-order rate constants determined experimentally for the oxidation of (A) Cu^{I}(*syn*-[14]aneS$_4$-diol) and (B) Cu^{I}(*anti*-[14]aneS$_4$-diol) with $Ni^{III}([14]aneN_4)$ as a function of the reciprocal concentration of the latter reagent (for data involving [Ni(III)] > 0.5 mM). The intercepts and slopes yield (A) $k_{2B} = (2.8 \pm 0.8) \times 10^4$ M^{-1} s^{-1} and $k_{RP} = (1.6 \pm 0.1) \times 10^2$ s^{-1} and (B) $k_{2B} = (8.4 \pm 3.8) \times 10^3$ M^{-1} s^{-1} and $k_{RP} = 50 \pm 4$ s^{-1}.

Plots of eq 8b for $[Ni^{III}([14]aneN_4)] > 0.5$ mM are shown for the two diol systems in parts A and B of Figure 7.[35] Both plots are linear and yield the following resolved values: for Cu^{I}(*syn*-[14]aneS$_4$), $k_{2B} = (2.8 \pm 0.8) \times 10^4$ M^{-1} s^{-1} and $k_{RP} = (1.6 \pm 0.1) \times 10^2$ s^{-1}; for Cu^{I}(*anti*-[14]aneS$_4$), $k_{2B} = (8.4 \pm 3.8) \times 10^3$ M^{-1} s^{-1}, and $k_{RP} = 50 \pm 4$ s^{-1}.

With an estimate of k_{2B} in hand, it is then possible to generate a "corrected" form of eq 8a in which the contribution of k_{2B} is taken into account

$$\frac{1}{k_{21} - k_{2B}} = \frac{[A_{Ox}]}{k_{RP}} + \frac{K_{PR}}{k_{2A}} \qquad (8c)$$

Plots of this "corrected" expression are illustrated in Figure 8 in which all $[Ni^{III}([14]aneN_4)]$ data are included. In both cases, the intercepts are statistically zero indicating that the contribution of the second-order term for pathway A is negligible over the range of reagent concentrations used. From the reciprocal slopes, we obtain k_{RP} values of $(1.6 \pm 0.6) \times 10^2$ and 47 ± 2 s^{-1} for Cu^{I}(*syn*-[14]aneS$_4$-diol) and Cu^{I}(*anti*-[14]aneS$_4$-diol), respectively, these values being identical with those obtained from the plots of eq 8b as anticipated. (The larger error in the k_{RP} value for Cu^{I}(*syn*-[14]aneS$_4$-diol) from the plot in Figure 8A is principally due to the fact that, for the larger values of [Ni(III)], the term $(k_{21} - k_{2B})$ represents the difference between two large numbers; thus, any experimental fluctuations in k_{21} are exaggerated in plots of this type.)

Shift in Preferred Reaction Pathway. Application of eq 6 to the resolved k_{2B} values for the $Cu^{I}L$ systems reacting with Ni(III) yields self-exchange rate constants characteristic of pathway

(32) For systems in which more than one term in eq 7 contributes to the observed kinetics, the value of $[A_{Ox}]$ must be kept constant during the course of any specific kinetic run so that the relative contributions of the first- and second-order processes remain constant. Since this requires maintaining a large excess of the counterreagent, the lowest concentration value which may be accessed is limited to about 10 times the smallest $Cu^{I}L$ concentration for which sensitive data can be obtained. (For thermodynamically unfavorable reactions, such as the reactions with $Ru^{III}(NH_3)_4bpy$, the minimum counterreagent concentration is further limited by the need to drive the reaction sufficiently far to the right to obtain resolvable data.) At the high concentration end, the solutions become nearly opaque. For the Ni(III) reactions, the maximum useful concentration range was found to be about 50-fold.

(33) Brunschwig, B. S.; Sutin, N. *J. Am. Chem. Soc.* **1989**, *111*, 7454–7465.

(34) Equation 8a is equivalent to the corresponding pseudo-first-order rate constant (k_{obsd}) expression used previously by Sykes and co-workers (where all terms in our eq 8 have been divided by $[A_{Ox}]$). As rewritten using our subscript designations, Sykes' equation is of the form: $1/k_{obsd} = (1/k_{RP}) + (K_{PR}/k_{2B}[A_{Ox}])$, where $k_{obsd} = k_{21}[A_{Ox}]$ (Al-Shatti, N.; Lappin, A. G.; Sykes, A. G. *Inorg. Chem.* **1981**, *20*, 1466–1469; eq 5).

(35) Independent plots of eqs 8a and 8b for each of the four series of data for the oxidation of Cu^{I}(*syn*-[14]aneS$_4$-diol) with $Ni^{III}([14]aneN_4)$ (Table 4) yielded slopes for the series II data which, relative to the other three series, were statistically rejectable by the Q test at the 98% confidence level: Rorabacher, D. B. *Anal. Chem.* **1991**, *63*, 139–146. Thus, only the three consistent series were utilized for the plots in Figures 7 and 8.

Table 13. Comparative Self-Exchange Rate Constants for Pathways A and B and Rate Constants for the R → P Conformational Change for $Cu^{II/I}$(*syn*-[14]aneS$_4$-diol), $Cu^{II/I}$(*anti*-[14]aneS$_4$-diol), and Related Systems at 25 °C and μ = 0.10 M

complexed ligand	log $k_{11(A)}$ (M^{-1} s^{-1})	log $k_{11(B)}$ (M^{-1} s^{-1})	log k_{RP} (s^{-1})	$k_{11(A)}/k_{11(B)}$
[14]aneS$_4$	3.88 ± 0.09[a,b]	−0.1 ± 0.2[a,c]	1.7 ± 0.1[a,d]	1×10^4
syn-[14]aneS$_4$-diol	3.4 ± 0.1[b]	−0.4 ± 0.3[c]	2.20 ± 0.02[d]	6×10^3
anti-[14]aneS$_4$-diol	4.3 ± 0.2[e]	−2.0 ± 0.4[c]	1.70 ± 0.03[d]	2×10^6
[13]aneS$_4$	5.50[b,f]	≈2.0[f,g]	≥2.3[f,h]	$\approx 3 \times 10^3$
[15]aneS$_4$	4.08[b,f]	≈2.2[f,g]	≤0.7[f,h]	$\approx 8 \times 10$

[a] Reference 2. [b] Value determined directly from NMR line-broadening measurements. [c] Mean calculated self-exchange rate constant from application of the Marcus relationship to cross-reaction rate constants obtained from the oxidation of $Cu^{I}L$ with Ni^{III}([14]aneN$_4$) (high concentration limit), $Ru^{III}(NH_3)_2(bpy)_2$ and Fe^{III}(4,7-Me$_2$phen)$_3$ as counter reagents. [d] Value obtained under limiting first-order conditions for the oxidation of $Cu^{I}L$ using Ni^{III}([14]aneN$_4$) as the counterreagent. [e] Value represents the mean self-exchange rate constant calculated from the application of the Marcus relationship to the cross-reaction rate constants obtained from the reduction of $Cu^{II}L$ with a variety of counterreagents. [f] Reference 4. [g] Value based on calculated self-exchange rate constant for reactions involving the largest potential barrier functions. [h] Estimate of limiting value.

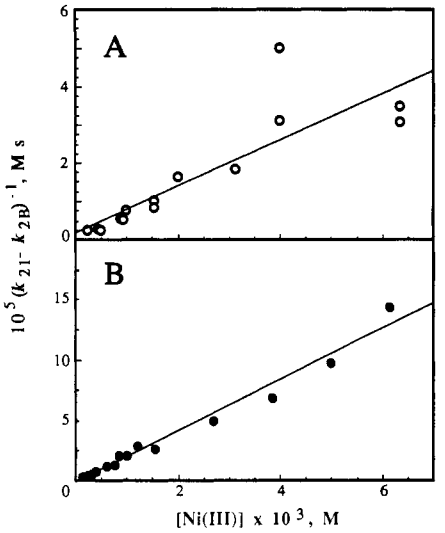

Figure 8. Plot of the "corrected" eq 8c for the "apparent" second-order rate constants obtained for the oxidation of (A) Cu^{I}(*syn*-[14]aneS$_4$-diol) and (B) Cu^{I}(*anti*-[14]aneS$_4$-diol) with Ni^{III}([14]aneN$_4$) as a function of the concentration of the latter reagent (using all data). The reciprocal slopes yield (A) k_{RP} = (1.6 ± 0.6) × 10^2 s^{-1} and (B) k_{RP} = 47 ± 2 s^{-1}.

B: $k_{11(B)}$ = 0.2 M^{-1} s^{-1} and 3.3 × 10^{-3} M^{-1} s^{-1} for the *syn*- and *anti*-diol systems, respectively (see "limiting" k_{11} values in Table 12). It is significant that these $k_{11(B)}$ values from the Ni(III) data are within experimental error of the k_{11} values generated from the kinetic studies in which $Ru^{III}(NH_3)_2(bpy)_2$ and Fe^{III}(4,7-Me$_2$phen)$_3$ were utilized as oxidants. This is consistent with our hypothesis that the $Cu^{I}L$ reactions with the latter two reagents are, indeed, proceeding via pathway B. For the previously studied $Cu^{II/I}$([14]aneS$_4$) system, the availability of ancillary rapid-scan cyclic voltammetric data[3b] has also made it possible to establish the fact that the $k_{11(Ox)}$ values obtained with these latter two reagents were consistent with the parameters for pathway B—that is, eq 7c applies. The fact that both $Ru^{III}(NH_3)_2(bpy)_2$ and Fe^{III}(4,7-Me$_2$phen)$_3$ have much larger values for the "potential barrier function", $K_{21}k_{22}$, than does Ni^{III}([14]aneN$_4$) is also consistent with the conclusion that these reagents react with all three $Cu^{I}L$ species exclusively by pathway B; that is, they have attained the limiting conditions implied by eq 7c even when very small concentrations of reagent are utilized.

Correlation of Electron-Transfer Behavior to Structural Changes. On the basis of the foregoing analysis of the *syn*- and *anti*-diol systems, the mean self-exchange rate constants for both pathways A and B ($k_{11(A)}$ and $k_{11(B)}$) as well as the rate constant for the R → P conformational change (k_{RP}) are tabulated in Table 13. Also included for comparison are the corresponding values for each of the three other Cu(II/I) systems for which this same set of rate constants has been previously evaluated.

It is noteworthy that both of the diol systems show significant differences when compared to $Cu^{II/I}$([14]aneS$_4$). The $k_{11(A)}$ value for the latter system is, in fact, intermediate between the values for the two diol systems. By contrast, the $k_{11(B)}$ value for the *syn*-diol is within experimental error of the parent compound while the *anti*-diol value is nearly 2 orders of magnitude smaller. Yet, for the k_{RP} value, it is the *anti*-diol system which is similar to $Cu^{II/I}$([14]aneS$_4$) while the *syn*-diol is 3-fold larger.

It is intriguing to note that the k_{RP} value for the *syn*-diol system is virtually identical to the corresponding value approximated for the [13]aneS$_4$ system. The crystal structures for both Cu^{II}(*syn*-[14]aneS$_4$-diol) and Cu^{II}([13]aneS$_4$) show the copper atom to be five-coordinate, perched above the S$_4$ plane. In the case of the latter system, reduction to the $Cu^{I}L$ species has been proposed to involve the breakage of a Cu–S bond in forming a tetrahedral coordination sphere.[4,7b] It is tempting to speculate that the Cu^{I}(*syn*-[14]aneS$_4$-diol) complex may also involve a ruptured Cu–S bond and that the transformation of R → P involves the reformation of this bond. By contrast, however, the $k_{11(ex)}$ value for this system has the largest activation enthalpy (and, yet, one of the least negative activation entropies) yet obtained among the Cu(II/I)–macrocyclic polythiaether complexes which have been examined to date, resulting in the smallest $k_{11(A)}$ value observed within this family.

It should be recognized, of course, that the crystal structures obtained for the Cu(II) complexes with [14]aneS$_4$, *syn*-[14]aneS$_4$-diol, and *anti*-[14]aneS$_4$-diol may not be directly indicative of the structures in solution. For example, alternative structures for the Cu^{II}(*anti*-[14]aneS$_4$-diol), for which the internal strain in the ligand is minimal, are illustrated in Figure 6, and similar alternative structures appear to be possible for the *syn*-diol complex in which two solvent molecules are coordinated to the copper. However, it is evident from the kinetic data in Table 13 that the substituent –OH groups must introduce significant variations in the preferred conformational geometries of the $Cu^{II}L$ and $Cu^{I}L$ species.

The observation that the limiting $k_{11(B)}$ value for $Cu^{II/I}$(*anti*-[14]aneS$_4$-diol) is more than $1^1/_2$ orders of magnitude smaller than the corresponding values for the other [14]aneS$_4$ systems indicates that species Q, the metastable Cu(II) complex which is presumed to approximate a tetrahedral geometry, is particularly unstable with the *anti* ligand. This factor, coupled with an accessible value of k_{RP} leads to the extended range of gated behavior observed for this system. Efforts to quantify the molecular mechanical constraints associated with the placement of substituents on the macrocyclic ligand are continuing.

Acknowledgment. This work was supported, in part, by Grant CHE-9218391 from the National Science Foundation. The authors wish to acknowledge the assistance and suggestions of Dr. Mohamad Ksebati in acquiring and interpreting the NMR data as well as the support of the Central Instrument Facility in the Chemistry Department at Wayne State University. The NMR spectrometer utilized in this work was purchased through an equipment grant from the National Science Foundation. Modifications to the stopped-flow spectrophotometer were funded with an unrestricted grant from ICI Americas.

Supplementary Material Available: Complete tables of NMR line-broadening data, kinetic data, supplemental crystallographic data, thermal parameters, and hydrogen atom parameters (13 pages). Ordering information is given on any current masthead page.